Catalysis Science & Technology

ROYAL SOCIETY OF CHEMISTRY

PAPER

View Article Online
View Journal | View Issue

Cite this: *Catal. Sci. Technol.*, 2020, **10**, 7262

Cobalt-containing zeolitic imidazole frameworks for C–H activation using visible-light redox photocatalysis†

Matthew E. Potter, ‡*[a] Cameron P. Ross,‡[ab] Diego Gianolio,[c] Ramon Rios[a] and Robert Raja *[a]

Received 24th May 2020,
Accepted 7th September 2020

DOI: 10.1039/d0cy01061h

rsc.li/catalysis

The activation of C–H bonds for carbon–carbon coupling reactions remains a challenge in organic synthesis. Visible light photocatalysis offers a unique opportunity to sustainably perform these reactions in a single-step, without the need for caustic reagents, and under ambient operating conditions. We utilize non-noble metals in the form of hybrid cobalt-based zeolitic imidazole frameworks, for the first time, to explore the structure–property correlations leading to the photocatalytic formation of C–C bonds. Combining *in situ* spectroscopy and theoretical simulations we can rationalize the photocatalytic efficacy of different frameworks. This led to an improved understanding of the nature of the photocatalytic active sites and associated reaction pathway.

1. Introduction

Alternative methods of chemical synthesis are required to meet government and industrial pledges to become carbon neutral by 2050. Several approaches are being explored including electrochemical and photochemical methods, and combinations thereof. Electrochemical C–H transformations are rapidly gaining interest,[1] where transition metal catalysts can achieve impressive yields under the correct conditions. However such systems still require significant electrical input which, in order to be sustainable, must derive purely from green energy sources. Further, due to the nature of the reaction, it is often challenging to recycle the electrolyte or incorporate a heterogeneous catalyst at an industrial scale.[1] In contrast, the light in photocatalysis can serve as both a heat and activation source. Many studies have been performed on titania-based catalysts, due to its availability and low cost.[2] Despite achieving high yields in a range of reactions, titania suffers from primarily using UV light, which constitutes only a fraction of the solar spectrum. This has commonly led to UV sources being used to stimulate photochemical reactions. So while titania is effective at absorbing the higher energy photons, its activity could be improved by modifying its band gap,[3] bringing it in-line with the solar spectrum. As such there is great interest in developing photocatalysts that can utilise visible light, allowing them to take advantage of solar energy. Currently there are few examples of wide-scale photochemical applications.[4,5] Photocatalysis is a growing area of organic synthesis, where the ability to form C–C bonds, with sunlight activating the substrate, derives from photosynthesis. As such, there is a desire to develop materials that can utilize visible light for a wider range of chemical transformations.[6,7] One process that could benefit from photocatalytic advancement is cross-dehydrogenative coupling (CDC). The CDC process provides an energy-efficient alternative to C–C bond formation, removing the need for multiple synthetic steps.[8] The photocatalytic aza-Henry reaction offers a sustainable alternative, whereby photons can be harvested to activate nitromethane and *N*-arylated tetrahydroisoquinolines to form a C–C bond from two sp^3 C–H species.[9–11] The nature of the active site and the reaction pathway must be well understood, thus *in situ* spectroscopy is pivotal to the design process in order to create an effective, recyclable photocatalyst.

Metal–organic frameworks (MOFs) consist of metal nodes or clusters, connected by organic linkers to form porous networks. MOFs are of great interest in photocatalysis, as their hybrid nature permits a range of synthetic modifications to tune catalytic performance.[12,13] Zeolitic imidazole frameworks (ZIFs), a subset of MOFs, are typically comprised of

[a] *Department of Chemistry, University of Southampton, Highfield Campus, Southampton, Hants, SO17 1BJ, UK. E-mail: M.E.Potter@soton.ac.uk, R.Raja@soton.ac.uk*
[b] *Institute of Chemical and Engineering Sciences (ICES), Agency of Science, Technology and Research (A*STAR), Neuros, 8 Biomedical Grove, Singapore 138665*
[c] *Diamond Light Source, Rutherford Appleton Laboratories, Harwell, Oxon, OX11 0FA, UK*

† Electronic supplementary information (ESI) available: Including physicochemical characterisation, further EXAFS analysis and details, stability measurements, proposed catalytic mechanism and reactant synthesis details. See DOI: 10.1039/d0cy01061h

‡ These authors contributed equally.

isolated cobalt(II) or zinc(II) ions, bridged by imidazole linkers to form a M(II)–Im–M(II) bond angle of 145°, analogous to zeolites.[14,15] ZIFs have shown promise in the photocatalytic reduction of CO_2,[16,17] and have potential in photochemical organic syntheses. Rationalizing their photocatalytic efficacy requires a combination of theoretical calculations[18] and *in situ* characterization techniques such as optical transient and X-ray transient absorption spectroscopy. Currently scarce few MOFs have been tested for the aza-Henry CDC reaction. Among these examples are Cu-based systems with H_2O_2 as an oxidant in a non-photocatalytic system,[19,20] and photocatalytic Se-containing MOFs (UiO-68 Se),[21] or UiO-67 MOFs with modified Ir/Rh linkers.[22] However to date there are no examples of MOFs based around first row transition metals for the aerobic photocatalytic aza-Henry CDC reaction. Preliminary studies showed that ZIF-67 is a promising photocatalyst due to a long-lived charge separated intermediate state.[23] In spite of this, most photocatalytic ZIF processes rely on a light-harvesting chromophore or dye.[12,13,16] In this study we probe the photocatalytic potential of two cobalt-containing ZIF species, ZIF-9 and ZIF-67 (Fig. S1†), which have different imidazole linkers and limiting pore diameters (ZIF-9: benzimidazole, 2.4 Å, ZIF-67: 2-methylimidazole, 3.4 Å).[24] These frameworks were selected to allow a direct comparison of two cobalt ZIFs with identical framework topology (sodalite; SOD), with similar hydrocarbon linkers. Therefore, any photocatalytic variances arise from the differences in the local structure associated with the cobalt site, due to the electronic and steric effects of the imidazole linker. By linking photocatalytic performance to the cobalt active site of the ZIF, for the first time, *via* a preliminary *in situ* X-ray adsorption spectroscopy (XAS) study, we will draw structure–property correlations towards designing improved photocatalytic materials for demanding aerobic C–C bond formations.

2. Experimental

2.1. ZIF synthesis

ZIF-9. ZIF-9 was synthesised using a previously reported method[25] cobalt(II) nitrate hexahydrate (1.11 g, 3.8 mmol) and benzimidazole (0.33 g, 2.8 mmol) were dissolved in DMF (50 mL) before heating to 130 °C for 48 hours. Once at room temperature the solution was filtered and washed with DMF (3 × 10 mL). Red and blue crystals were collected and left in a drying oven. The solid was ground before centrifuging in chloroform (3 × 10 mL). The supernatant was decanted each time before removing the solvent *in vacuo*. The blue solid was dried under vacuum at 100 °C for 6 hours.

ZIF-67. ZIF-67 was synthesized from a reported procedure[26] involved dissolving 2-methylimidazole (5.5 g, 67 mmol) in water (20 mL). Cobalt(II) nitrate hexahydrate (0.45 g, 1.5 mmol) in water (3 mL) was added and the mixture left stirring for 6 hours. The purple precipitate was collected by centrifugation, washing with water (2 × 10 mL) and methanol (2 × 10 mL). The solid was dried at 100 °C for 6 hours under vacuum.

2.2. Physicochemical characterization

SEM. Scanning electron microscopy images were obtained by gold sputter coating MOF samples loaded onto silica wafers and visualized with a JEOL JSM-6500F field emission scanning electron microscope.

BET. N_2 physisorption measurements were performed at liquid nitrogen temperature, by first degassing the samples under vacuum. Surface area was determined by nitrogen adsorption–desorption isotherms using Micromeritics ASAP 2020, calculated using the BET method.

XRD. Powder XRD was undertaken on a Bruker AXS D2 Phaser with Cu radiation (wavelength = 1.5406 Å). The range scanned was dependent on the expected framework, whilst a step of 0.02° was used for all scans.

UV/vis. (DR) UV–vis measurements were conducted using a Shimadzu 2600 spectrometer with integrated sphere. Reference standard was $BaSO_4$, obtaining a range from 200–850 nm.

TGA. Analysis was completed using a Netzsch Libra TG 209 F1 with a ramp rate of 10 °C min^{-1}, air flow of 50 mL min^{-1}, He flow of 10 mL min^{-1} for balance, with a temperature range of 30–900 °C.

ICP. ICP measurements were conducted on a Varian Vista MPX CCD simultaneous axial ICP-OES instrument, based at MEDAC Ltd. Laboratories.

2.3. XAS, XANES simulations and density of states calculations

XAS data was collected at B18 at the Diamond Light Source, Harwell. The ZIF photocatalysts were diluted with cellulose to form a pellet 13 mm in diameter, mounted on a sample holder. The experimental hutch was darkened and XAS data collected at a scan rate of 3 minutes per scan for 10 scans to give the 'dark' scans. The solar simulator (placed ~25 cm away to mimic reaction conditions and temperature) was turned on and data collected for a further 10 scans, allowing the system to equilibrate before 10 '*hν*' scans were collected and averaged. The light was then turned off and 'dark' scans were recollected to evaluate the effect of beam damage on the sample. Measurements were referenced to a metallic Co(0) foil. XAFS data processing and EXAFS analysis were performed using IFEFFIT with the Horae package (Athena and Artemis).[27] The amplitude reduction factor, S_0^2, was derived from EXAFS data analysis of the known reference compound, Co(0) metallic foil.

XANES simulations were performed using the *ab initio* full-multiple scattering (FMS) code FEFF 8.4 (ref. 28) on a cluster using experimental atomic coordinates for ZIF-9 and ZIF-67 obtained from cif files.[14,15] The simulations are performed using self-consistent potential calculations (SCF) in the muffin-tin approximation with 15% overlap between the muffin tins and with Hedin–Lundqvist energy dependent exchange correlation potential with a −4 eV edge shift. The radius for the SCF was chosen at 4.5 Å to include 41 atoms and radius for the FMS calculations was chosen at 7 Å large

enough to include 86 atoms. XANES was calculated up to 6 $Å^{-1}$ and an increasing step in energy corresponding to a constant step in *k*-space of 0.05 $Å^{-1}$ for the whole spectrum with exception of a small area near the edge where a constant energy step of 0.2 eV has been used. Projected density of states has been calculated for all atomic orbitals in a the range from −15 to +25 eV around the edge with a step of 0.2 eV.

2.4. Photocatalytic measurements of PhTHIQ to $MeNO_2$–PhTHIQ

PhTHIQ (0.11 mmol) and catalyst (10 wt%) were stirred in nitromethane (1 mL), with mesitylene as an internal ^1H NMR standard, for 6 h at 40 °C. The light source was an Oriel 150 W Xe short arc lamp, equipped with a AM1.5G solar simulator filter, placed 25 cm away from the reaction mixture, (solely responsible for generating the 40 °C reaction temperature), giving a power output of 50 mW cm^{-2}. The spectra was modified with a 515 nm longpass filter (515FCS, Knight Optical) to remove UV light. The mixture was analyzed using ^1H NMR, on a Bruker AV400 FT-NMR spectrometer in $CDCl_3$. Chemical shifts for proton and carbon spectra are reported on the delta scale in ppm, referenced to tetramethylsilane (TMS). Conversion and yield were calculated relative to a mesitylene peak (2.2 ppm, 9H), and then compared with a starting material (PhTHIQ) peak at 3.00 ppm (2H) and a product ($MeNO_2$–PhTHIQ) peak at 5.55 ppm (1H). Exact peak positioned varied between substrates **1a–1f**, however the same assigned peaks were used. All repeated experiments were found to be within ±3 mol%, as such we adopt this as our error for all catalytic measurements. For details on reactant synthesis please refer to the ESI.†

'Blank' was performed in the absence of any photocatalyst. 'ZIF-9 N_2' was performed in an analogous fashion to typical experiments, except the system was degassed with nitrogen for 1 hour prior to the reaction to remove any air from the system. 'ZIF-9 Dark' was performed, with the sample being shielded from any light and heated to 40 °C using an oil bath for 6 hours. 'Cobalt formate' was performed so that the amount of cobalt was identical to ZIF-9, to show the influence of a cobalt salt.

3. Results and discussion

3.1. Confirming the framework integrity

The framework integrity of the ZIF photocatalysts were confirmed using an array of physicochemical techniques. ZIF-9 was phase pure with no impurities detected (Fig. S2†). It had inaccessible pores due to trapped DMF (Fig. S3†), and crystalline particles with a narrow size distribution of 5–10 μm (Fig. 1) in good agreement with the literature.[25] ZIF-67 was also phase pure and showed surface areas in agreement with the literature (Fig. S2 and S3†), with scanning electron microscopy (SEM) the system formed particles in the range of 100–400 nm.[26,29] Thermogravimetric analysis showed a greater mass loss (Fig. S4†) in ZIF-9 than ZIF-67, due to the larger organic linker of ZIF-9 (benzimidazole). ZIF-67 shows a rapid mass loss after 400 °C, while ZIF-9 shows a more gradual loss starting at 250 °C, likely due to the removal of trapped DMF in the pores.[25,26,29] Finally ICP showed our experimental cobalt loading was in good agreement with the theoretical values (Table S1†), further confirming the integrity of both ZIF species.[14,15,25,26,29,30] The interaction of the ZIF samples with visible light was probed with UV/vis spectroscopy (Fig. 2 and S5†). Both ZIFs show a broad band between

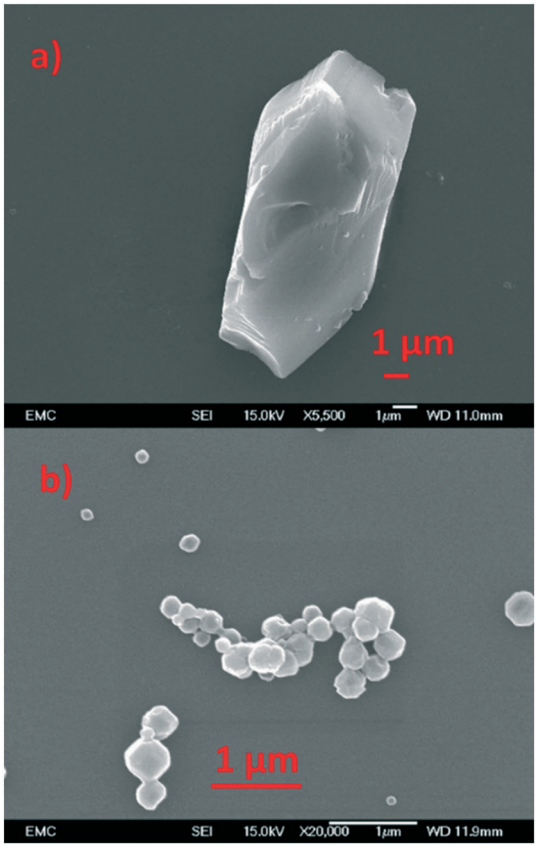

Fig. 1 SEM images showing the particle sizes of a) ZIF-9 and b) ZIF-67.

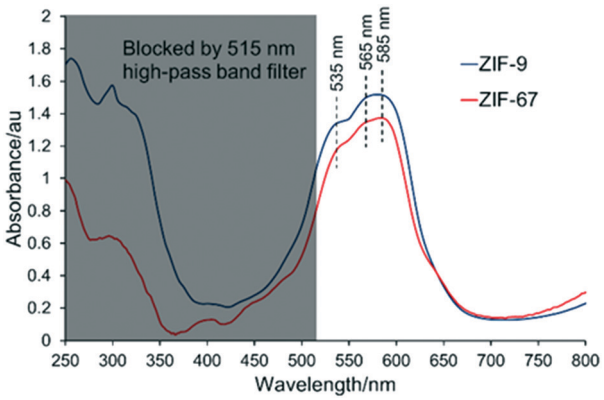

Fig. 2 UV/vis spectra of ZIF-9 and ZIF-9, highlighting the presence of isolated tetrahedral cobalt(II) and the influence of the 515 nm longpass filter.

500 and 600 nm, which is a combination of three signals at 535, 565 and 585 nm, assigned as $^4A_2(^4F) \rightarrow {}^4T_1(^4P)$, $^4A_2(^4F) \rightarrow {}^4T_1(^4F)$ and $^4A_2(^4F) \rightarrow {}^4T_2(^4F)$ d–d transitions respectively.[30,31] A cobalt–oxygen MLCT (metal to ligand charge transfer) at 250–300 nm is also seen, which is typical of Co(II) tetrahedral species.[30,32] The combination of these two features is indicative of isolated tetrahedral Co(II). Given the stringent selection rules, UV/vis cannot always provide a holistic understanding of the whole system. For example many researchers have highlighted LMCT in cobalt ZIFs between 550–650 nm,[33] though such features are typically quite broad and hidden by the intense d–d transitions. However, greater detail can be achieved when combining UV/vis spectroscopy with XAS.

From this data we estimate the band gap energy of the systems to be similar at 3.6 and 3.7 eV for ZIF-9 and ZIF-67 respectively, in the range predicted by DFT findings, which also show the band gap of ZIF-67 is higher than that of ZIF-9.[34]

3.2. XAS spectroscopy to probe the cobalt site

To explore the potential for photocatalytic activity for these ZIFs, *in situ* XAS data was collected under 'dark' and '*hν*' conditions for ZIF-67 and ZIF-9 (Fig. S6†). The EXAFS data and models for both are in excellent agreement with the expected crystallographic structure (Table S2, Fig. S6–S10†).[35,36] For both ZIF-9 and ZIF-67, cobalt exists in a tetrahedral environment, with a first coordination sphere of four nitrogen atoms, at 2.00 Å (±0.01). Although within error, under '*hν*' conditions subtle changes did occur in the XANES region (Fig. 3), with both pre-edges moving to slightly lower energy values. This may be indicative of Co(II) being promoted to a higher energy state, such as Co(II)*, or only a small percentage of Co(II) being reduced to Co(I). Density of States (DoS) theoretical simulations confirm the origin of the four features seen in the XANES region of both ZIF-9 and ZIF-67. The initial pre-edge feature at 7709 eV is due to a Co(1s) → Co(3d) transition with tetrahedral symmetry, as seen by the significant Co(d) contribution (Fig. 4 and S11†).[35–37]

The pre-edge is attributed to the Co(1s) → Co(4p) continuum with electron shakedown (7718 eV), terminating at 7727 eV, as Co(p) character occurs in this region.[35–37] The features at 7727 and 7731 eV are shown to have some C(p), N(p) and Co(p) character (Fig. 4 and S11†), thus the nature of the surrounding ligands influences these features. Subtracting the 'dark' from the '*hν*' spectra allowed for a more critical consideration of the influence of the light source (Fig. S5†). We note that the differences observed between the 'dark' and '*hν*' states are small. Though these differences are of similar magnitude to previous literature work.[23] It is possible that these spectral changes may be the result of thermal broadening due to the heat of the lamp, hence DoS findings are necessary to assign these features. ZIF-9 showed only very subtle signs of beam damage, with the initial and final dark spectra showing excellent agreement (Fig. S12A†). We note that ZIF-67 shows more noticeable changes (Fig. S12B†), though these

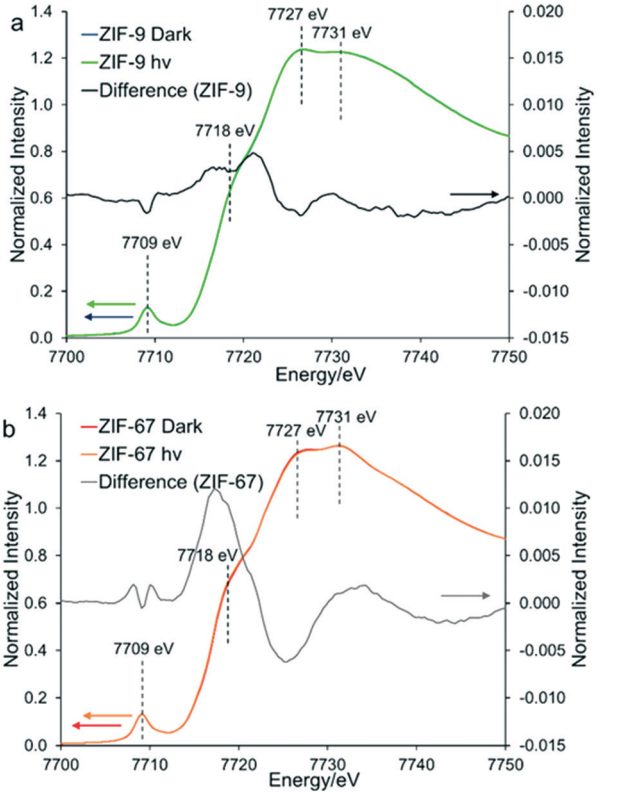

Fig. 3 Normalised XANES data highlighting the difference in the cobalt environment under both 'Dark' and '*hν*' conditions for a) ZIF-9 and b) ZIF-67. Note, the similarities between 'Dark' and '*hν*' spectra mean they are essentially super-imposed on this scale. Difference spectra are calculated by subtracting the 'Dark' spectra from the '*hν*'.

are more dramatic and distinct to the changes seen on photoactivation.

Under '*hν*' conditions the pre-edge of ZIF-67 shifts to a lower energy value, indicative of increased electron density (Fig. 3b) and partial reduction of Co(II), with electrons logically originating from the methyl-imidazole linker *via* a ligand-to-metal charge transfer (LMCT).[23]

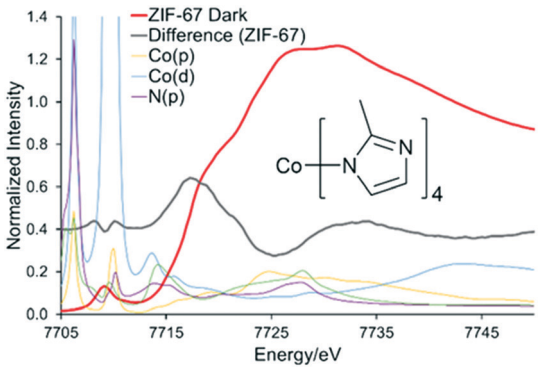

Fig. 4 DoS simulation results for ZIF-67, from the crystallographic structure of ZIF-67, showing the contributions from each orbital set. The difference spectrum is scaled by a factor of 20 and incremented by 0.4 for ease of observation.

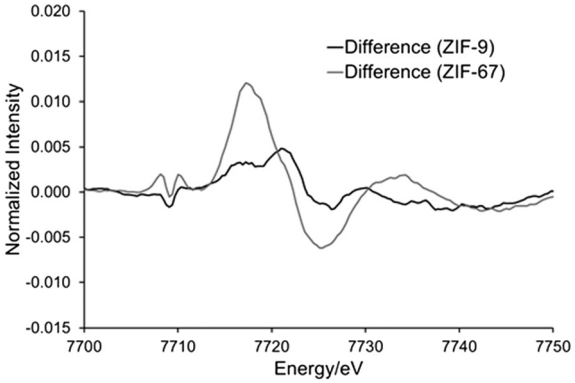

Fig. 5 Comparing the difference spectra of ZIF-9 and ZIF-67 between dark and *hν* XAS spectra.

This is in agreement with the DoS findings (Fig. 4 and S11†) as the maxima of the difference spectra coincides with the Co(p) system, suggesting increased electron density in these orbitals. While the minima coincides with the N(p), suggesting decreased electron density in these orbitals. This has previously been linked to an elongation of the Co–N bonds,[23] however this was not seen in our EXAFS model (Table S2†), where all changes were within the errors generated, due to the similarities in the EXAFS region (Fig. 5 and S6†). ZIF-9 does not show as significant a change in the pre-edge energy (Fig. 5), thus retains the Co(II) character on exposure to the light source, suggesting the LMCT does not occur to the same extent. In contrast, the ZIF-67 shows a more significant change on exposure to light in the XANES region (Fig. 5). This is likely due to the extended resonance structure of the aromatic ring of benzimidazole, and the bulkier framework, limiting the motion of the electrons and atoms. However, the positive inductive effect of the methyl group in ZIF-67 has a greater capacity for pushing electrons onto the cobalt atom upon photocatalytic excitation, leading to a greater shift in the XANES (Fig. 5).

3.3. Photocatalytic aza-Henry CDC reaction

These samples were tested in the photocatalytic aza-Henry reaction of *N*-phenyl-1,2,3,4-tetrahydroisoquinoline (PhTHIQ) with nitromethane to 1-(nitromethyl)-*N*-phenyl-1,2,3,4-tetrahydroisoquinoline ($MeNO_2$–PhTHIQ), simultaneously activating two C–H bonds to form a new C–C bond.[5–8,38] To exclusively utilize visible light, a 515 nm longpass filter was employed, blocking the UV contribution while maximizing the absorption of low-energy visible light by the ZIF species (Fig. S5†).

In all cases $MeNO_2$–PhTHIQ was the primary product, as shown by the yield, however some degradation and over-oxidation productions such as isoquinolines may also form, which are accounted for by the disparity in conversion and yield. ZIF-9 was shown to be a superior photocatalyst, achieving a $MeNO_2$–PhTHIQ yield of 84 mol% after 6 hours, compared to 55 mol% for ZIF-67 (Table 1 and Fig. S13†). Both ZIFs outperformed the cobalt formate salt (41 mol%, Table 1 and Fig. S13†) which was also tested as a homogeneous cobalt(II) species, which one may expect from cobalt leaching.

The difference in activity between ZIF-9 and ZIF-67 was confirmed *via* a kinetic study (Fig. 6), where ZIF-9 consistently outperformed ZIF-67. The pore apertures of ZIF-9 and ZIF-67 (2.4 and 3.4 Å respectively) will be too small to accommodate PhTHIQ, thus surface sites must play a dominant role in this reaction. Earlier we showed ZIF-67 has more cobalt that ZIF-9 (Table S1†), and smaller particles (Fig. 1), two factors which should boost the activity of a purely surface-catalysed reaction. However, as ZIF-9 is the more active, despite the larger particle size and less cobalt, then we can conclude the precise coordination environment of the cobalt, and its response to photoexcitation, is the main determinant in photocatalytic activity.

To prove the reaction was photocatalytic, control experiments were performed (Table 1 and Fig. S13†). Removing light (Table 1, entry 5) showed inferior product yields.

Table 1 Photocatalytic activity of cobalt-containing ZIFs and control reactions for the aza-henry CDC reaction

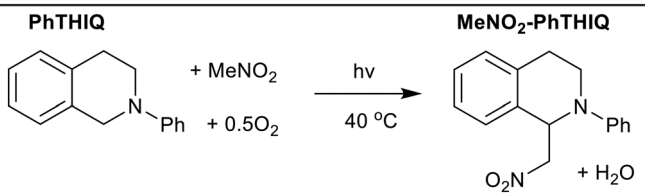

System	Conversion/mol%[a]	Yield/mol%[b]
ZIF-9	90	84
ZIF-9 4th recycle	90	82
ZIF-67	59	55
Cobalt formate	51	41
ZIF-9 dark	17	16
ZIF-9 N_2	0	0
Blank	8	8

Reaction conditions: PhTHIQ (0.11 mmol) and catalyst (10 wt%) were stirred in nitromethane (1 mL), with mesitylene as an internal ^{1}H NMR standard, for 6 h at 40 °C, using a solar simulator with a 515 nm longpass filter. [a] Conversion of reactant. [b] Yield of product. Errors are estimated as ±3 mol% based on repeated measurements.

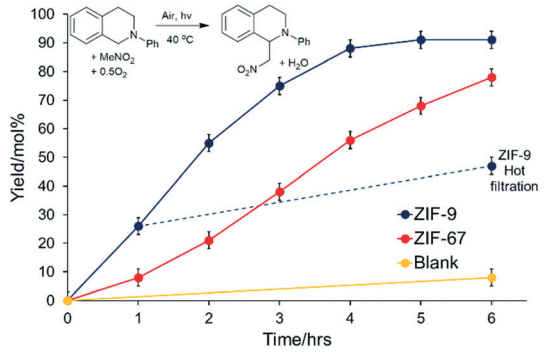

Fig. 6 Kinetic photocatalytic data for the aza-Henry reaction of nitromethane with PhTHIQ to $MeNO_2$–PhTHIQ. Reaction conditions: PhTHIQ (0.11 mmol) and catalyst (10 wt%) were stirred in nitromethane (1 mL), with mesitylene as an internal ^{1}H NMR standard, for 6 h at 40 °C, using a solar simulator with a 515 nm longpass filter. Note: yields for the ZIF species are higher than for a single measurement as the reaction mixture was opened to the air to sample each hour, refreshing the oxidant.

Therefore light is pivotal to the reaction, with heat alone having little effect (Table 1 and Fig. S13†). ZIF-9 was completely inactive with light under an inert (N_2) environment (Table 1, entry 6), confirming oxygen is necessary for the reaction to proceed. Finally, a blank reaction showed minimal activity with oxygen and light without solid catalyst (Table 1, entry 7), demonstrating that the ZIFs act as photocatalysts. The stability of ZIF-9 was proven over multiple cycles (Table 1, entry 2), with the catalyst being collected by filtration prior to reuse between cycles. The $MeNO_2$–PhTHIQ was consistent between the first (84 mol%) and after a fourth recycle (82 mol%), and still significantly higher than cobalt salt. This consistency suggests the framework species is still intact, and that minimal (if any) leaching occurs and confirms the recyclability of the heterogeneous ZIF-9 system, supporting the stability of the material. Further, a hot filtration experiment was performed after 1 hour and showed minimal increase in yield, in line with the blank reaction (Fig. 6).

Modified versions of the substrate were prepared and tested, varying the electron density of the aromatic ring (Table 2), for studying substrate scope. The substituents strongly influenced the product yield, which was highest for electron-donating groups (R = 4-OMe, 92 mol%), though decreased as the substituent became increasingly electron withdrawing (R = 2-F, 39 mol%). This observation supports the proposed mechanism, where electron donating substituents will help to stabilize the radical cation intermediate, favouring the generation of the final reactive imine (Fig. 7 and S13†).[39]

As the specific photocatalyst has a strong influence on the reaction efficacy, the pivotal step of the proposed mechanism is likely part of the photocatalytic cycle of the cobalt species (Fig. 7 and S13†). Given that light plays a crucial role in the reaction, we argue that the first step must be photocatalytic. We submit the first step; (A) is the initial photocatalytic excitation of Co(II) into a higher energy Co state. This is likely due to the d–d transitions witnessed in the UV/vis (Fig. 2), which could create an electron hole in a lower-lying orbital. However this could also involve oxidation of Co(II) to Co(III), which is commonly seen in a range of catalytic materials.[40] It is also possible this may occur by disproportionation of a Co(II) pair to a Co(I) and Co(III) species. Our current spectroscopic analysis is presently unable to confirm which pathway is active, however given the importance of light and oxygen, photoactivation must occur. A separate reaction was performed where 3.3 mmol (30 mol%) of DABCO was added to the system, serving as a singlet oxygen scavenger. This saw the yield of $MeNO_2$–PhTHIQ drop to 21 mol% after 6 hours, as opposed to 84 mol% without the DABCO (Tables 1 and 2). This suggests that the formation of singlet oxygen may also play a role in this mechanism. Though its removal was not sufficient to completely kill the reaction.

It is well known that for the CDC reaction to occur the reagent must undergo oxidation,[23,41] requiring the catalyst itself to be reduced; step (B). This may occur by an excited Co(II)* performing a single electron transfer to the reagent, resulting I Co(I), generating an amine cationic radical from PhTHIQ in the process. Though the transition between Co(II) and Co(III) is more common, the photocatalytic reduction of Co(II) to Co(I) has been reported.[23,41] It is also possible that

Table 2 Substrate screening for ZIF-9 for the photocatalytic aza-Henry CDC reaction

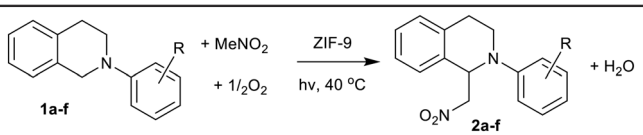

R	Product	Conversion/mol%[a]	Yield/mol%[b]
H	**2a**	90	84
4-Me	**2b**	91	91
4-OMe	**2c**	98	92
4-Cl	**2d**	64	64
4-CF_3	**2e**	57	47
2-F	**2f**	42	39

Reaction conditions: PhTHIQ (0.11 mmol) and catalyst (10 wt%) were stirred in nitromethane (1 mL), with mesitylene as an internal ^{1}H NMR standard, for 6 h at 40 °C, using a solar simulator with a 515 nm longpass filter. [a] Conversion of reactant (**1a–f**). [b] Yield of product (**2a–f**).

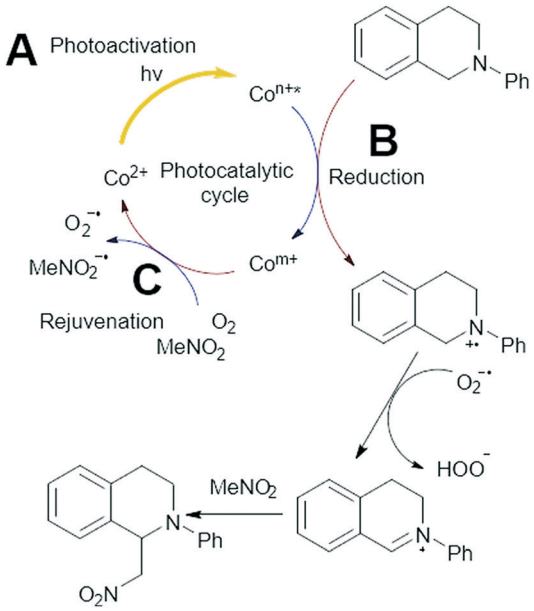

Fig. 7 Suggested photocatalytic cycle for the aza-henry CDC reaction.

this step could also involve the reduction of Co(III) to Co(II).[40] Again, we cannot conclude the precise mechanism, but submit that a reduction step is required. Finally, step (C) occurs; the rejuvenation of the catalyst by either oxygen or nitromethane to close the photocatalytic cycle. The XANES analysis suggests that a LMCT occurs upon photochemical excitation,[23] increasing the electron density on the cobalt. This is more noticeable in ZIF-67 (Fig. 5) than ZIF-9, despite ZIF-9 being the more active photocatalyst. We believe that step (B) is the rate limiting step in the catalytic cycle, due to ZIF-9 being the better photocatalyst with a less pronounced LMCT transfer. The LMCT will increase electron density on the cobalt, which will make the cobalt less oxidising due to weaker interactions with other electrons. UV/vis spectroscopy has already provided an insight into step (A), with greater range of visible s wavelengths that ZIF-9 can absorb, relative to ZIF-67, therefore offering more opportunities to form the excited state. However, the broadening of the UV/vis signal for ZIF-9 was only slight, and the band gaps are similar, which is unlikely to have a drastic influence on the catalysis. As step (B) is likely the rate-determining step in this cycle, it should be the main consideration for rational design of future visible light heterogeneous catalysts for this reaction.

Conclusions

By judicious selection of the imidazole linker, we have demonstrated that the photocatalytic efficacy of heterogeneous solids can be tuned to create an improved photocatalyst in a demanding C–H activation reaction, utilizing visible light ($\lambda > 515$ nm). Through a combination of UV/vis, XAS spectroscopy and theoretical simulations, we have shown that the reduction step and the range of light adsorbed to activate the cobalt site play a pivotal role in this reaction. This can be controlled and enhanced through astute selection of the imidazole linker, with benzimidazole (ZIF-9) preventing the LMCT seen with 2-methylimidazole (ZIF-67), leading to ZIF-9 being a superior photocatalyst. These findings open up possibilities for a wider range of functionalized imidazole linkers to be experimentally and computationally screened for this reaction, towards developing an optimized photocatalytic species. Controlling the precise coordination environment of the cobalt species in the ZIF-9 framework, confers the benefits of a stable, recyclable heterogeneous photocatalyst for effecting sustainable organic transformations.

Conflicts of interest

There are no conflicts to declare.

Acknowledgements

The work was funded by the EU's Horizon 2020 program under grant number 720783 (MULTI2HYCAT) and EPSRC (UK) (EP/N013883/1). CPR was funded through a joint University of Southampton and A*STAR, Singapore scholarship. The beamtime was carried out at B18, Diamond Light Source under proposal SP-15151 *via* the UK Catalysis Hub Beamtime Allocation Group.

Notes and references

1 C. Ma, P. Fang and T. S. Mei, *ACS Catal.*, 2018, **8**, 7179–7189.
2 M. Pelaez, N. T. Nolan, S. C. Pillai, M. K. Seery, P. Falaras, A. G. Kontos, P. S. M. Dunlop, J. W. J. Hamilton, J. A. Byrne, K. O'Shea, M. H. Entezari and D. D. Dionysiou, *Appl. Catal., B*, 2012, **125**, 331–349.
3 S. Higashimoto, *Catalysts*, 2019, **9**, 201.
4 N. S. Lewis, *Science*, 2016, **351**, aad1920.
5 C. G. Silva, R. Juárez, T. Marino, R. Molinari and H. Garcia, *J. Am. Chem. Soc.*, 2011, **133**, 595–602.
6 M. Oelgemöller, *Chem. Rev.*, 2016, **116**, 9664–9682.
7 D. M. Schultz and T. P. Yoon, *Science*, 2014, **343**, 1239176.
8 C. S. Yeung and V. M. Dong, *Chem. Rev.*, 2011, **111**, 1215–1292.
9 A. G. Condie, J. C. González-Gómez and C. R. J. Stephenson, *J. Am. Chem. Soc.*, 2010, **132**, 1464–1465.
10 D. Ravelli and M. Fagnoni, *ChemCatChem*, 2012, **4**, 169–171.
11 L. D. Shirley, V. Ceban, M. Meazza and R. Rios, *ChemistrySelect*, 2016, **1**, 13–15.
12 T. Zhang and W. Lin, *Chem. Soc. Rev.*, 2014, **43**, 5982–5993.
13 A. Dhakshinamoorthy, A. M. Asiri and H. Garcia, *Angew. Chem., Int. Ed.*, 2016, **55**, 5414–5445.
14 K. S. Park, Z. Ni, A. P. Côté, J. Y. Choi, R. Huang, F. J. Uribe-Romo, H. K. Chae, M. O'Keefe and O. M. Yaghi, *Proc. Natl. Acad. Sci. U. S. A.*, 2006, **103**, 10186–10191.
15 R. Banerjee, A. Phan, B. Wang, C. Knobler, H. Furukawa, M. O'Keefe and O. M. Yaghi, *Science*, 2008, **319**, 939–943.
16 S. Wang, W. Yao, J. Lin, Z. Ding and X. Wang, *Angew. Chem., Int. Ed.*, 2014, **53**, 1034–1308.

17 S. Yan, S. Ouyang, H. Xu, M. Zhao, X. Zhang and J. Ye, *J. Mater. Chem. A*, 2016, **4**, 15126–15133.
18 R. Grau-Crespo, A. Aziz, A. W. Collins, R. Crespo-Otero, N. C. Hernández, L. M. Rodriguez-Albelo, A. R. Ruiz-Salvador, S. Calero and S. Hamad, *Angew. Chem., Int. Ed.*, 2016, **55**, 16012–16016.
19 X. L. Yang, C. Zou, Y. He, M. Zhao, B. Chen, S. Xiang, M. O'Keefe and C. D. Wu, *Chem. – Eur. J.*, 2014, **20**, 1447–1452.
20 S. L. Zhu, S. Ou, M. Zhao, H. Shen and C. D. Wu, *Dalton Trans.*, 2015, **44**, 2038–2041.
21 W. Q. Zhang, Q. Y. Li, Q. Zhang, Y. Lu, H. Lu, W. Wang, W. Zhao and X. J. Wang, *Inorg. Chem.*, 2016, **55**, 1005–1007.
22 C. Wang, Z. Xie, K. E. deKrafft and W. Liu, *J. Am. Chem. Soc.*, 2011, **133**, 13445–13454.
23 B. Pattengale, S. Yang, J. Ludwig, Z. Huang, X. Zhang and J. Juang, *J. Am. Chem. Soc.*, 2016, **138**, 8072–8075.
24 M. Erkartal, U. Erkilic, B. Tam, H. Utsa, O. Yazaydin, J. T. Hupp, O. K. Farha and U. Sen, *Chem. Commun.*, 2017, **53**, 2028–2031.
25 Q. Li and H. Kim, *Fuel Process. Technol.*, 2012, **100**, 43–48.
26 J. Qian, F. Sun and L. Qin, *Mater. Lett.*, 2012, **82**, 220–223.
27 B. Ravel and M. Newville, *J. Synchrotron Radiat.*, 2005, **12**, 537–541.
28 A. L. Ankudinov, B. Ravel, J. J. Rehr and S. D. Conradson, *Phys. Rev. B: Condens. Matter Mater. Phys.*, 1998, **58**, 7565–7576.
29 C. Mottillo, Y. Lu, M. H. Pham, M. J. Chliffe, T. O. Do and T. Friščić, *Green Chem.*, 2013, **51**, 2121–2131.
30 Z. Öztürk, J. P. Hofmann, M. Lutz, M. Mazaj, N. Z. Logar and B. M. Weckhuysen, *Eur. J. Inorg. Chem.*, 2015, **9**, 1625–1630.
31 S. Dzwigaj and M. Che, *J. Phys. Chem. B*, 2006, **110**, 12490–12493.
32 V. Kurshev, L. Kevan, D. J. Parillo, C. Pereira, G. T. Kokotailo and R. J. Gorte, *J. Phys. Chem.*, 1994, **98**, 10160–10166.
33 M. Wang, J. Liu, C. Guo, X. Gao, C. Gong, Y. Wang, B. Liu, X. Li, G. G. Gurzadyan and L. Sun, *J. Mater. Chem. A*, 2018, **6**, 4768–4775.
34 K. T. Butler, C. H. Hendon and A. Walsh, *Faraday Discuss.*, 2017, **201**, 207–219.
35 F. Hillman, J. M. Zimmerman, S. M. Paek, M. R. A. Hamid, W. T. Lim and H. K. Jeong, *J. Mater. Chem. A*, 2017, **5**, 6090–6099.
36 A. Moen and D. Nicholson, *Chem. Mater.*, 1997, **9**, 1241–1247.
37 R. Sarangi, J. Cho, W. Nam and E. I. Solomon, *Inorg. Chem.*, 2011, **50**, 614–620.
38 S. A. Girard, T. Knauber and C. J. Li, *Angew. Chem., Int. Ed.*, 2014, **53**, 74–100.
39 H. Bartling, A. Eisenhofer, B. König and R. M. Gschwind, *J. Am. Chem. Soc.*, 2016, **138**, 11860–11871.
40 C. J. Wu, J. J. Zhang, Q. Y. Meng, T. Lei, X. W. Gao, C. H. Tung and L. Z. Wu, *Org. Lett.*, 2015, **17**, 884–887.
41 T. Lazarides, T. McCormick, P. Du, G. Luo, B. Lindley and R. Eisenberg, *J. Am. Chem. Soc.*, 2009, **131**, 9192–9194.